Design of Non-Depleting Electrolyte Additive to Prolong the Cycle Life of Practical Lithium-Sulfur Batteries

Authors: Xiaowei Wang[1+], Saurabh Parab[2+], Ganesh Raghavendran[1], Bing Han[1], Bhargav Bhamwala[1], Shuang Bai[2], Alex Liu[1], Weikang Li[1], Matthew Miyagishima[1], Shen Wang[1] and Ying Shirley Meng[1,3]*

Affiliations:

1, Department of Nanoengineering,
University of California San Diego,
9500 Gilman Dr, La Jolla, CA 92093, USA.

2, Program in Materials Science and Engineering,
University of California San Diego,
9500 Gilman Drive – MC 0418,
La Jolla, CA 92093-0418, USA

3, Pritzker School of Molecular Engineering,
The University of Chicago,
Chicago, IL 60637, USA.

[+]These authors contributed equally: Xiaowei Wang, Saurabh Parab.

Lead contact:
Professor Dr. Ying Shirley Meng
E-mail: shirleymeng@uchicago.edu

SUMMARY

Battery technology is pivotal in addressing energy efficiency and environmental sustainability challenges. Lithium-sulfur (Li-S) batteries feature promising high energy density and sustainability, but are hindered by a short cycle life under lean lithium and electrolyte conditions. A critical hurdle for Li-S batteries is the selection of an optimal electrolyte solution, crucial for controlling effective polysulfide electrochemical reactions. The conventional ether-based Li-S electrolyte, consisting of lithium bis(trifluoromethanesulfonyl)imide (LiTFSI) and lithium nitrate ($LiNO_3$), frequently suffers from $LiNO_3$ depletion in high-energy-density applications. To address the capacity decay in Li-S batteries caused by $LiNO_3$ depletion, this investigation introduces 2-nitrophenol lithium (NPL) as an alternative. By incorporating 25

mM NPL and 1 M LiTFSI in a 1,3-dioxolane/1,2-dimethoxyethane (DOL/DME) solvent, NPL mediates polysulfide oxidation during charging and prevents polysulfide corrosion, therefore improving Li retention and plating behavior. This results in Li-S batteries with NPL achieving 310 cycles, significantly surpassing the 75 cycles observed with traditional $LiNO_3$-containing electrolytes using lean lithium anode. Pouch cells incorporating NPL exhibit stable cycling over 80 cycles, maintaining 75% of their capacity. The molecular structure of NPL prevents decomposition and facilitates interaction with polysulfides to minimize corrosion, positioning it as a strong substitute for $LiNO_3$. This highlights NPL as a promising solution for extending the lifespan of Li-S batteries.

INTRODUCTION

The pressing challenges of climate change and energy depletion have driven humanity towards adopting a lifestyle that emphasizes high energy efficiency and environmental sustainability. Battery technology emerges as a pivotal solution, providing strategies to address power generation fluctuations and mitigate pollution, thereby reducing the carbon footprint in human society. The ongoing advancements in portable devices and the swift expansion of electric vehicles (EVs) are driving an increasing need for batteries possessing specific traits, such as heightened energy densities, reduced costs, and extended lifespans.[1] Lithium-sulfur (Li-S) batteries are at the forefront of next-generation energy storage technologies, distinguished by their high energy density. This density results from the high specific capacities of the sulfur cathode and lithium anode, combined with a lightweight design and environmental sustainability. Such features hold tremendous potential for high-energy-density applications, including electric vehicles and aerospace, as well as for sustainable energy storage solutions.[2]

Despite their promising potential, Li-S batteries confront several intrinsic challenges. These include the insulating nature of cathode materials, such as S/Li_2S, and the volume expansion of both cathode and anode electrodes. Additionally, they suffer from the dissolution of polysulfide intermediates during the charge and discharge process, along with the instability of the lithium metal anode.[3] These challenges significantly limit the cycle life of Li-S batteries, especially impeding the advancement of practical high-energy-density lithium-sulfur batteries that utilize reduced lithium and electrolyte content.[3,4] Over the past few decades, extensive endeavors have been undertaken to address cathode design,[5-8] separator modification,[9] lithium engineering technologies (surface stabilization and alloying),[10,11] and electrolyte solution enhancements (additives and redox mediators)[12]. These strategies have demonstrated considerable improvements in Li-S battery performance. Despite these achievements, a

3

substantial gap remains between laboratory demonstrations and practical applications, especially in terms of energy density and battery longevity. Current research effort is directed towards enhancing the cycle life of Li-S batteries with high energy density.

The redox chemistry of lithium-sulfur (Li-S) batteries in their liquid state presents several critical challenges, notably concerning the electrolyte's compatibility with electrodes, polysulfide solvation, and the deposition of polysulfide on the cathode substrates. Effective electrolyte selection is pivotal, serving not only as an ionic conductor but also actively participating in lithium and sulfur conversion reactions.[2,13] The electrolyte's composition significantly influences various aspects such as lithium stripping/plating control, dendrite growth inhibition, solid electrolyte interphase (SEI) passivation, and side reactions confinement.[12] In conventional ether-based Li-S electrolytes, like the baseline electrolyte (consisting of 1 M LiTFSI and 2wt.% $LiNO_3$ in a 1:1 volume ratio of DOL and DME), lithium polysulfides are moderately dissolved, forming the catholyte with high specific capacity.[12,14] Besides, $LiNO_3$ mediates polysulfide oxidation on the cathode side and passivates the Li metal anode.[12] However, $LiNO_3$ depletion during charge/discharge poses a significant challenge,[15-17] especially in high-energy-density Li-S batteries with limited electrolyte.[3,18] Exploring alternatives to $LiNO_3$ is crucial, as current additives derived from nitrate anion (NO_3^-) are still prone to decomposition.[19,20] Additionally, while effective polysulfide solvation enhances sulfur utilization and reaction kinetics, it introduces the challenging "shuttle effect," leading to lithium corrosion and reduced cycle life. Researchers typically focus on modifying the electrolyte composition to suppress polysulfide dissolution, which compromises energy density since lithium polysulfide intermediates are charge carriers delivering energy.[21,22] Hence, strategically engineering non-reactive polysulfide structures is essential to protect the Li metal anode, ensuring the viability of high-energy-density Li-S batteries.[21]

4

In this study, we designed and synthesized an aromatic nitro-functionalized compound, 2-Nitrophenol Lithium (NPL), to replace the depleting LiNO$_3$. The electrolyte, comprising 1 M LiTFSI in a DOL/DME (v/v=1:1) mixture solvent, incorporates a low concentration (25 mM) of NPL as an additive. NPL, with its six-member ring stabilization structure, binds to polysulfides, mediating their oxidation without any severe decomposition observed with LiNO$_3$. Utilizing high-performance liquid chromatography (HPLC), we quantified significant LiNO$_3$ depletion and minor NPL consumption in Li-S battery electrolytes under conditions of limited lithium and electrolyte. Besides, the NPL-polysulfide interaction inhibits polysulfide reactions with the Li metal anode, resulting in improved Li inventory retention and bulky Li plating behavior compared to baseline electrolytes. Li-S batteries using the NPL (25 mM) based electrolyte exhibit significantly extended longevity for 310 cycles compared to a limited lifespan of 75 cycles with baseline electrolytes containing LiNO$_3$ (~400 mM). Additionally, single-layer pouch cells (~0.1 Ah) with the NPL electrolyte demonstrate stable cycling for approximately 80 cycles, achieving a high capacity retention of 75%. These enhancements arise from the decomposition-inhibiting conjugated stable structure of NPL and its interaction with polysulfides, reducing polysulfide corrosion on the Li anode in high-energy-density Li-S batteries. This study introduces an alternative to LiNO$_3$ that features a robust bonding structure, which inhibits the decomposition of crucial additives. This advancement paves the way for the development of Li-S electrolytes capable of supporting high polysulfide concentrations. Consequently, it ensures the extended lifespan of Li metal anodes without self-degradation.

RESULTS

The design of electrolyte additive in Li-S batteries.

The LiNO$_3$ depletion of Li-S conventional electrolyte (1 M LiTFSI in DOL/DME, v/v=1/1, 2wt.% LiNO$_3$) has prompted the development of alternative additives. Prior work has

5

been focused on developing nitrate anion (NO_3^-) derivatives that can be decomposed to passivate Li anode.[19,20] However, nitrate anion is readily reduced and oxidized during sulfur redox reactions.[17,19,20,23] This results in $LiNO_3$ decomposition impairing its effect on mediating the polysulfide oxidation process, which causes battery failure ultimately. Thus far, the cycle life of Li-S batteries is highly dependent on the electrolyte amount when using the baseline electrolyte. Nitrate anion sustains N-O bond cleavage by accepting electrons to be reduced easily forming nitrite anion (NO_2^-) (**Figure 1a**), which is also thermodynamically favorable irreversible process (**Table S1**, more discussion is shown in the Supporting Information 'Theoretical calculation of $LiNO_3$ decomposition' session).[23] It is important to design new chemical compounds with robust bonding structures without N-O cleavage. In this study, the nitro group is chosen as an alternative to the nitrate anion, and a benzene ring is introduced for generating a stable aromatic nitrophenol lithium salt, specifically 2-nitrophenol lithium (NPL). This selection is based on the established intramolecular bonding between the nitro oxygen (nitro-O) and phenol lithium (phenol-Li) depicted in **Figure 1a**. More detailed information regarding the NPL synthesis is supplied in the Supporting Information, 'the synthesis of 2-nitrophenol lithium (NPL)' session. The synthesis and purity of NPL were evidenced by the Nuclear Magnetic Resonance (NMR) spectra in **Figure S1** and the Inductively Coupled Plasma Optical Emission spectroscopy Mass Spectroscopy (ICP-MS) result in **Figure S2** of NPL.
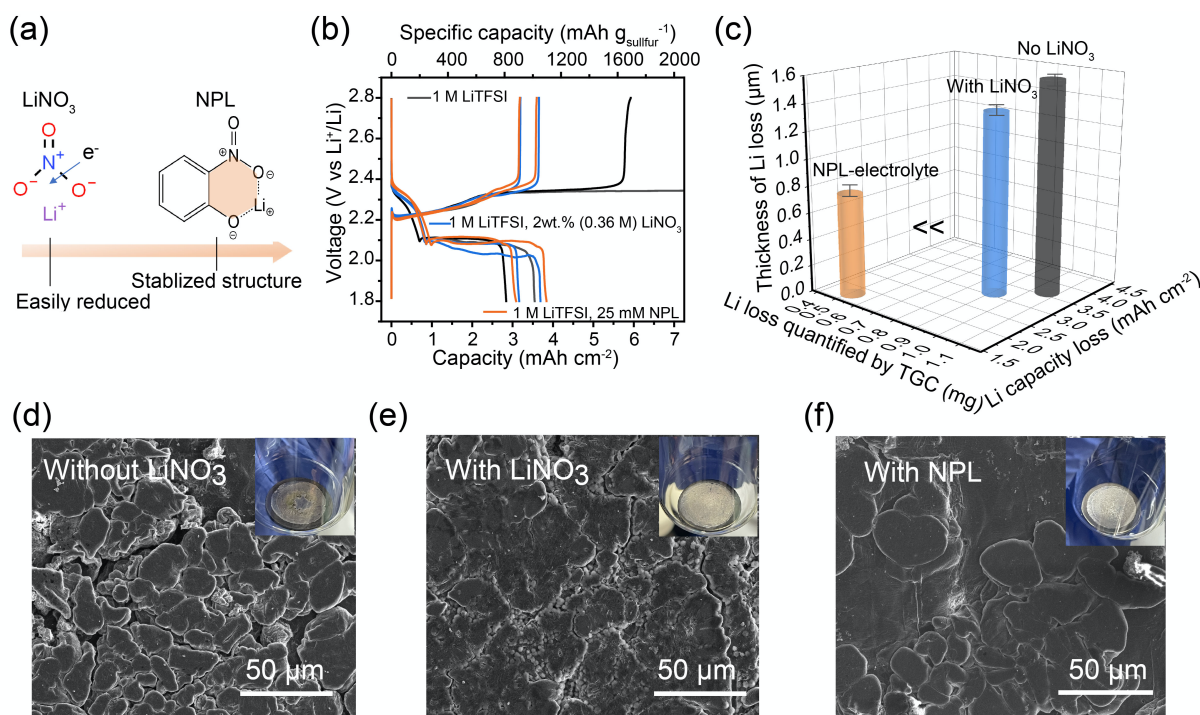
Figure 1. The design of additives and the analysis Li anode in various electrolytes. (a) The schematic of LiNO$_3$ decomposition and its alternative of NPL; (b) The voltage profiles of C-S cathodes paired with 100 µm Li foils in formation cycles at 0.05 C (1 C = 1000 mA g^{-1}) in various electrolytes with an electrolyte-to-sulfur (E/S) ratio of 8 µl mg^{-1}; (c) The Li inventory loss in thickness, mass, and capacity after formation cycles quantified by TGC; (d, e, and f) The large-scale cryo-SEM images of Li foils after formation cycles and the insets of the digital images of the Li disassembled from the cells in the three electrolytes.

Figure 1b presents the typical voltage profiles of the Li-S batteries at 0.05 C using a carbon-sulfur (C-S) cathode (the preparation details are given in the Supporting Information 'The preparation of C-S cathodes' session) and three electrolytes: 1M LiTFSI in DOL/DME (No LiNO$_3$), the baseline (with LiNO$_3$), and 1M LiTFSI in DOL/DME with 25 mM NPL (NPL-electrolyte). The ionic conductivities for NPL-electrolyte and baseline electrolyte are approaching (**Table S2**). The Li-S cells using the electrolyte without LiNO$_3$ suffer from the severe over-charging problem originating from incomplete polysulfide oxidation that causes shuttle corrosion to Li anode simultaneously.[14,15,17,21] By contrast, NPL and LiNO$_3$ both act as functional additives to mediate the polysulfide oxidation during the charge process of the corresponding Li-S cells. Notably, the C-S cathode delivers slightly higher specific capacity in

7

the NPL-electrolyte than baseline electrolyte indicating a more efficient polysulfide conversion from Li_2S to S.

Meanwhile, titration gas chromatography (TGC)[24] was employed to quantify the Li inventory loss in the corresponding Li-S cells after the formation cycles at 0.05 C (**Figure 1b**) using the three electrolytes mentioned above (**Figure 1c**). After the formation cycles in all three different electrolytes depicting similar areal discharge capacities and utilization, the lithium losses were compared. The data in **Figure 1c** reveal that without any additive, the Li-S cells experienced a Li inventory loss exceeding 1.06(+/-0.01) mg. The introduction of $LiNO_3$ slightly reduced this loss to 0.91(+/-0.01) mg. Remarkably, with the addition of NPL, the loss was further decreased to 0.51(+/-0.01) mg. In Li-S batteries, Li loss typically results from the polysulfide shuttling effect.[14,25] Therefore, the addition of NPL significantly mitigates the shuttling effect, outperforming $LiNO_3$.

Further, **Figure 1d-f** show the large-scale cryogenic scanning electron microscopy (Cryo-SEM) images and the optical images (insets) of the Li foils tested in the above electrolytes, presenting the difference in the Li stripping and plating processes. Specifically, polysulfide shuttle causes Li particle pulverization (**Figure 1d**) and $LiNO_3$ additive sacrifices to passivate the Li metal to yield bulky Li deposition (**Figure 1e**).[15] Notably, the NPL-electrolyte enables bulky and dense Li deposition indicating inhibited polysulfide reaction with Li (**Figure 1f**), which is evidenced by the minor S peak of EDX spectra of the plated Li foil in the NPL electrolyte compared to the other two electrolytes (**Figure S3**).

The surface chemistry of Li anode in the electrolytes.

To elucidate the effects of electrolytes on the Li metal anode, X-ray photoelectron spectroscopy (XPS) with depth profiling was performed to investigate the surface chemical information of the deposited Li metal in the Li-S cells after charging processes in the baseline and NPL electrolytes (**Figure 2a and 2b**). We identified that the solid-electrolyte-interface (SEI)

8

components in both electrolytes closely match those reported in previous studies.[24,26] Li_2S and Li_2O emerge as the predominant inorganic compounds. Meanwhile, the organic portion comprises alkyl oxide (R-O-Li) and poly-ethers, which stem from the decomposition of DOL/DME ether solvents and Li salts.[27] In the nitrate-based baseline electrolyte, a decrease in the intensity of (C-C-O)n, C=O, and R-O-Li bonds suggests a reactive layer on the Li surface, as seen in **Figure 2a.** This layer's presence is confirmed by peaks at 532.1 eV, 531.2 eV, and 530.2 eV in O 1s. Additionally, peaks for C-O at 285.8 eV and C-C at 284.6 eV in C 1s further support this finding, as shown in **Figure S4**. The inorganic SEI components feature a dominant Li_2O peak at 528.2 eV[26] and a Li_2S peak at 159.8 eV[28]**,** as shown in **Figure 2a**. These peaks indicate a thick reactive layer on the Li surface after Li plating in the baseline electrolyte. This suggests the presence of an unavoidable polysulfide shuttle and a parasitic solvent reaction with the Li metal anode. By sharp contrast, in the NPL electrolyte treated sample, the intensity of Li_2O peak decreases, along with the shrinking peaks of the organic species for the case of the NPL electrolyte. The Li_2S peak primarily resides in the very outer layer of the Li surface, as shown in **Figure 2b**. This indicates a thinner reactive layer on the Li plated in the NPL electrolyte (compared to the baseline), resulting from inhibited polysulfide reactions and reduced solvent/salt decomposition.
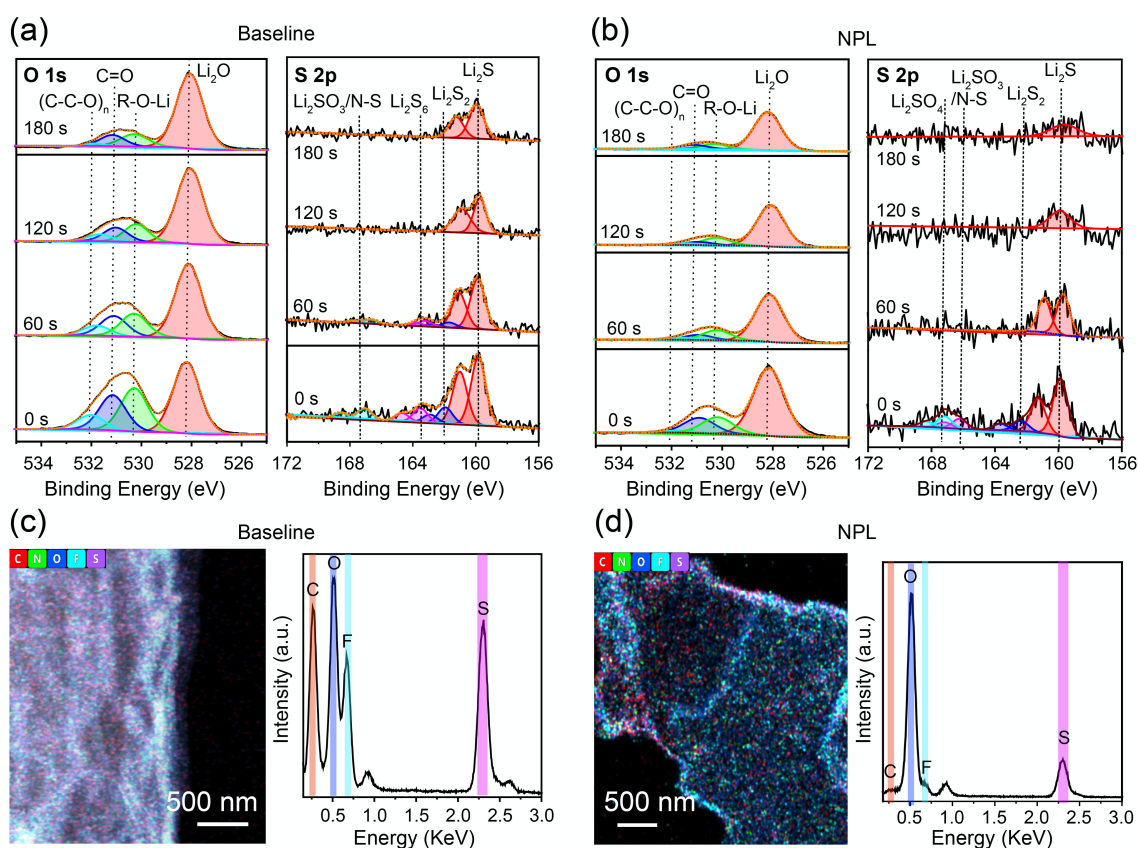
9

Figure 2. The surface chemical characterization of the Li anodes in the baseline and NPL electrolytes using the depth profiling XPS. The XPS depth-profiling spectra of O 1s and S 2p of Li foils after formation cycles in the baseline electrolyte (a) and the NPL electrolyte (b); The Cryo-TEM images with EDX spectra of Li redeposited after charge process in the baseline electrolyte (c) and the NPL electrolyte (d).

To further validate the inhibition of polysulfide reactions in the NPL electrolyte, we obtained localized Li grain information. This was done using low-electron-dose cryogenic scanning transmission electron microscopy (Cryo-STEM). The STEM Energy-dispersive X-ray spectroscopy (EDX) elemental mapping was performed for a few key elements of SEI components, such as C, N, O, F, and S. **Figure 2c and 2d** present the EDX mapping of the Li metal plated on Cu grids inserted in Li-S full cells using the baseline and NPL electrolytes based on a same C-S cathode. The related voltage profiles and EDX elemental weight percentage statistics are provided in the **Figure S5** and **Table S3**. As a result, the Li plated in the baseline electrolyte shows evident peaks of C, O, F, and S representing SEI compounds distributed on Li surface. The O and S peaks are notably dominant, which is also reflected by

10

the XPS depth profiling results. For the case of plated Li in the NPL electrolyte, O peak still exists but S peak and other elemental peaks are minor, showing that polysulfide reaction is much inhibited. The mechanism on how NPL inhibits the polysulfide shuttle will be further explored in the next section.

DISCUSSION

The interaction between polysulfide and NPL.

In LiNO$_3$-based electrolytes, polysulfide oxidation is facilitated during the charge process,[15] but the reduction reaction of LiNO$_3$ is thermodynamically inevitable forming nitrite anion (NO$_2^-$) species giving negative Gibbs free energy (**Table S1**). Cyclic voltammetry (CV) was used to monitor any side reaction of the electrolyte additives using a very small scan rate of 0.02 mV s^{-1} as shown in **Figure 3a**. In CV, the electrolyte with NPL demonstrates typical sulfur redox peaks. The similar current intensity between the anodic and cathodic peaks suggests good reversibility of sulfur electrochemistry. In contrast, using a LiNO$_3$-containing electrolyte results in poor symmetry of sulfur redox peaks (indicating poor reversibility) and evident reduction peaks, as shown in **Figure S6**. Notably, the decrease in overpotential with increasing scan numbers is primarily due to the reduction in anodic peak potentials. This indicates the NPL effect in mediating polysulfide oxidation during the charging process, as shown in **Figure 3a**.

Therefore, it is of great significance to pinpoint the role of NPL during the S redox chemistry with the existence of polysulfide. **Figure 3b** presents the ultraviolet-visible (UV-vis) spectra of the chemically prepared Li$_2$S$_6$/DME solution, NPL/DME solution, NPL-Li$_2$S$_6$/DME mixture solution (1:1, molar ratio) and the DME solvent with the optical images of the sample solutions (**Figure 3b**, inset). Specifically, there are typical UV-Vis adsorption peaks at 410 nm for Li$_2$S$_6$[14,29] and 445 nm for NPL,[30] while the NPL-Li$_2$S$_6$ mixture sample shows blueshift referring to NPL (445 nm to 425 nm) suggesting the interaction site of -NO$_2$ group.
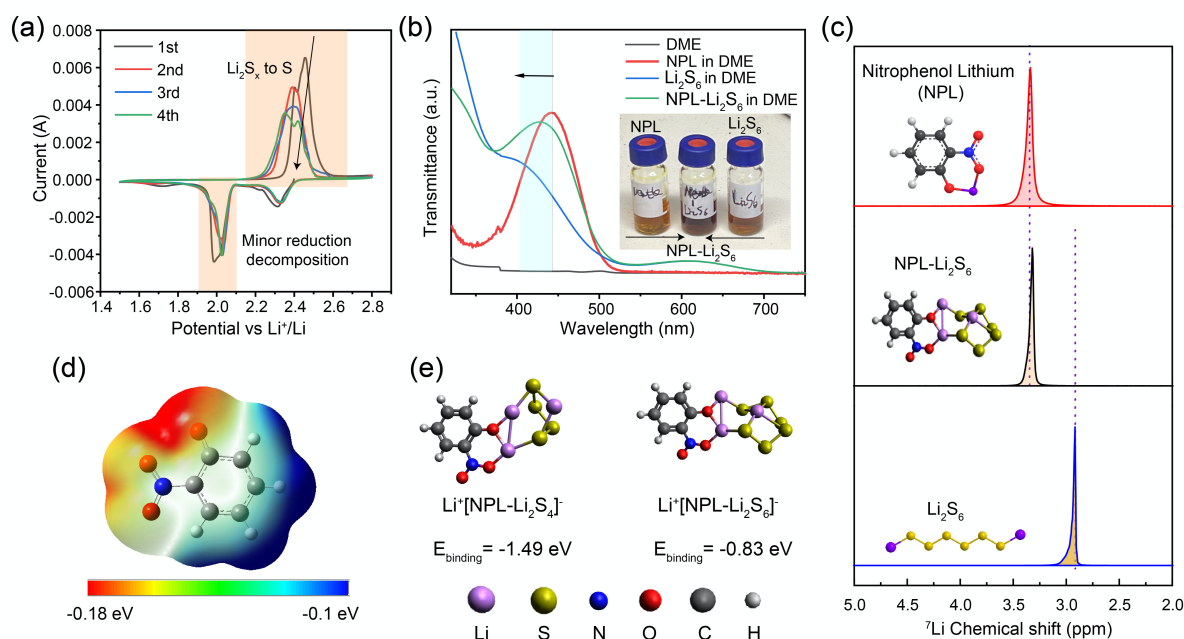
11

Figure 3. The investigation of NPL and polysulfide interaction. (a) The Cyclic voltammetry of C-S cathode in the NPL electrolyte at a scan rate of 0.02 mV s^{-1}; (b) The UV-Vis spectra of the solvent, NPL, Li$_2$S$_6$ and NPL-Li$_2$S$_6$ mixture (inset of the HPLC vials that contains the samples); (c) The ^{7}Li NMR of NPL, Li$_2$S$_6$ and the mixture; (d) Average Local Ionization Energy of NPL with the scale bar from -0.18 eV to -0.1 eV, red Area represents the point of electrophilic attack; (e) The binding energies and structures of NPL-Li$_2$S$_x$.

Electrostatic potential (ESP) mapping was done to map the electron density of the NPL anion (nitrophenolate ion) (**Figure 3c**), which shows the most reactive site for electrophilic addiction is between the functional nitro and phenol groups consistent with the UV-Vis results in **Figure 3b**. Combined with the ESP results (**Figure S7a**), the interacted polysulfide (Li$_2$S$_4$, and Li$_2$S$_6$)-NPL complexes of Li$^+$[NP-Li$_2$S$_4$]$^-$ and Li$^+$[NP-Li$_2$S$_6$]$^-$ were proposed and the proposed structures (**Figure S7b**) were optimized using Gaussian (**Figure 3d**). More had been discussed in the Supporting Information, 'The theoretical study of NPL-polysulfide binding structures' session. The calculated binding energies of -1.49 eV and -0.83 eV for Li$^+$[NP-Li$_2$S$_4$]$^-$ and Li$^+$[NP-Li$_2$S$_6$]$^-$ respectively offers insight into the complexing mechanism of NPL interacting with polysulfide. The proposed interaction is further validated by the ^{7}Li NMR spectra of NPL, Li$_2$S$_6$ and the mixture showing the chemical environmental evolution of Li

12

atoms (**Figure 3e**). The chemically-prepared Li_2S_6 sample and NPL feature chemical shift peaks at 2.95 ppm and 3.35 ppm, while the NPL-Li_2S_6 mixture has an obvious ^7Li peak shift to 3.30 ppm verifying the Li atom complexation of polysulfide with NPL (**Figure 3e**).

The performance evaluation of NPL.

To avoid the impact of electrode materials, the electrochemical behavior of the as-prepared NPL additive was evaluated by using the conventional carbon-sulfur (C-S) cathodes (**Figure S8**) with mere S electrochemistry. The cathodes present a sulfur areal loading of ~3.5 mg cm^{-2}, paired with thin lithium foil (100 μm) in CR2032 coin cells. The C-S cathodes deliver typical voltage profiles of Li-S batteries in both the NPL and baseline electrolytes (**Figure S9**) using an electrolyte-to-sulfur (E/S) ratio of 10 μl mg^{-1}, which shows the conventional sulfur redox chemistry utilized for energy storage. **Figure 4a** showcases the cycling stability of C-S cathodes with two different electrolytes. It highlights Li-S cells in the NPL electrolyte (25 mM NPL), which maintain 70% capacity after 310 cycles, starting from an initial capacity of 850 mAh g^{-1}. In contrast, cells in the baseline electrolyte containing $LiNO_3$ (~400 mM) exhibit a shorter cycle life of 75 cycles and with a lower initial capacity of 750 mAh g^{-1}. Moreover, the baseline Li-S cells experience significant capacity decay after 75 cycles, marking an inflection point (circled out in **Figure 4a**), along with overcharging issues as shown in **Figure S10**. This is attributed to incomplete polysulfide oxidation, suggesting the depletion of the $LiNO_3$ reservoir. As a result, the associated Li anode faces increased exposure to polysulfides that are not converted to elemental sulfur. Thus, a substantial sulfur loss of approximately 80.1% indicates the deterioration of the sulfur cathode. Additionally, severe polysulfide corrosion leads to significant degradation of the Li anode, resulting in a 47.00% loss of Li^0 inventory. These findings were quantified using thermogravimetric analysis (TGA) and titration gas chromatography (TGC)[24], as shown in **Figure S11** and **Table S4**.

By contrast, Li-S cells in the NPL electrolyte present much slow capacity decay after extended cycling. This benefits from more efficient sulfur electrochemistry supported by a well-maintained NPL additive reservoir, rendering a stable cathode with 31.25% sulfur retention (**Figure S11**) and a well-preserved anode with 34.58% Li^0 inventory loss (**Table S4**). To compare the consumption rate of Li-S electrolyte additives, such as $LiNO_3$ and NPL, we employed High-Performance Liquid Chromatography-Ultraviolet Spectroscopy (HPLC-UV). Both $LiNO_3$ and NPL are UV active chemical compounds[31], making them distinguishable from other electrolyte components such as LiTFSI, DME, and DOL through a suitable mobile gradient, Consequently, this method enables the quantification of the exact additive concentration both at the beginning and after the end of cycling. Using the external standards in DME/DOL, the HPLC-UV standard calibration curves for both NPL and $LiNO_3$ were obtained, as depicted in **Figure S12**. The sample preparation and analysis are provided Supporting Information, 'The quantification of the additives in Li-S electrolytes' session. Moreover, the quantified concentration was re-calculated to obtain the real concentration in the Li-S cells. **Figure 4b** and **Figure S13**, which display the corresponding HPLC chromatograms, reveal a significant depletion of $LiNO_3$ by 91% in baseline Li-S cells after 200 cycles, as shown in **Figure 4a**. This finding underscores the issue of $LiNO_3$ decomposition in conventional Li-S batteries.[12,15] However, NPL boasts a high retention of 75% after long cycling of 310 cycles, suggesting that the NPL is not susceptible to a sacrificial mediation process[15] like $LiNO_3$ for polysulfide oxidation. This is attributed to the robust aromatic chemical structure of NPL to resist decomposition and the NPL-polysulfide interaction to bypass the self-reduction. Notably, NPL still shows a consumption rate of 25% based on the small concentration of 25 mM after long cycling, which might be due to the inevitable passivation of Li anode to form SEI components like $LiNO_3$.[17]
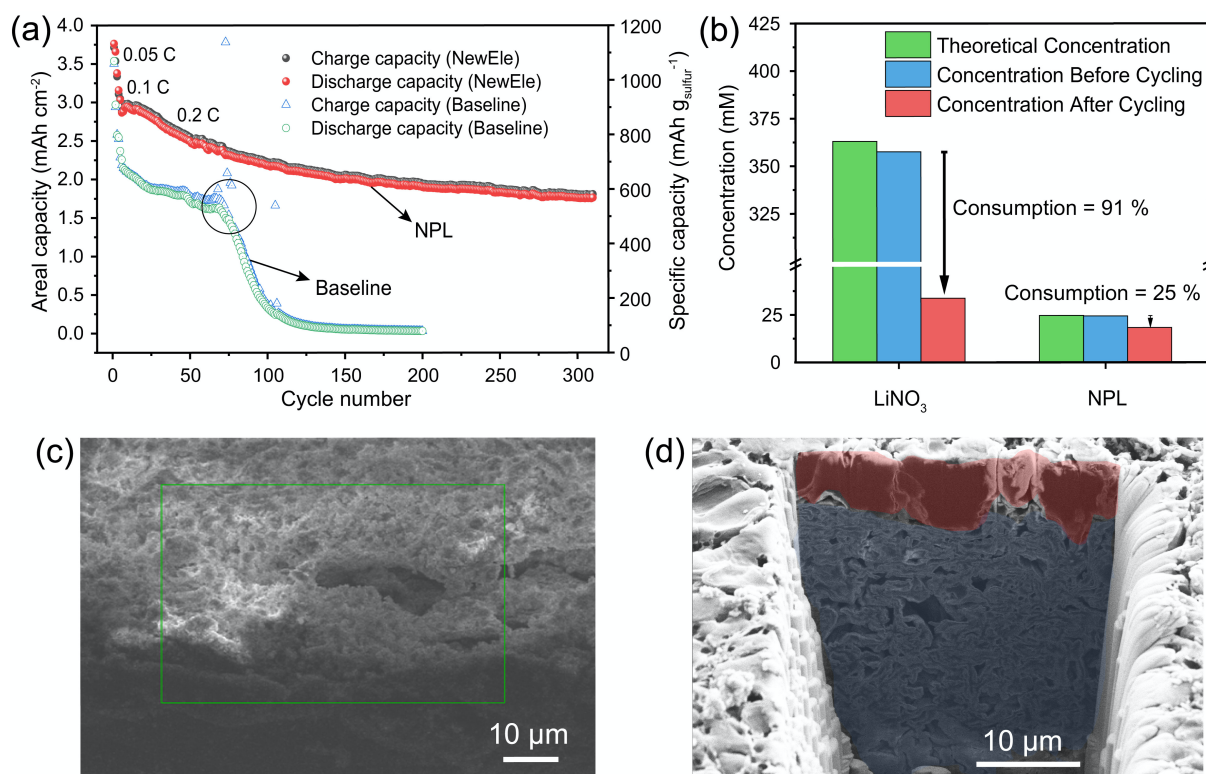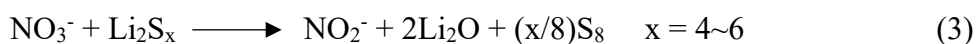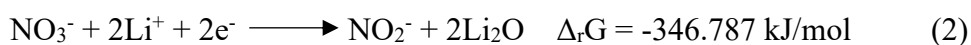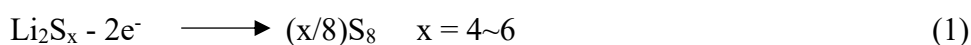
14

Figure 4. Electrochemical performance evaluation and the post-mortem analysis. (a) The cycling behavior of C-S cathode in the NPL electrolyte and baseline electrolyte using thin lithium foil (100 μm); (b) The HPLC-UV spectra of $LiNO_3$ in the baseline electrolyte before and after cycling; (c) The cycled Li anode in the baseline electrolyte showing severe pulverization (cross-section view); (d) The cryo-FIB image of the cycled Li anode in the NPL electrolyte.

As-discussed above regarding the Li anode protection, the NPL electrolyte is proved to inhibit the polysulfide reaction with Li (**Figure 2**). Therefore, the post-mortem analysis was conducted to investigate Li anode integrity after cycling. There is severe pulverization of Li anode after cycling in the baseline electrolyte, thus, it failed to undergo ion-beam milling using cryogenic focused ion beam (Cryo-FIB). The cross-section view under Cryo-SEM clearly shows severe polysulfide corrosion of the Li anode (**Figure 4c**). However, the cycled Li anode from the NPL-based Li-S cells preserves bulk Li deposition after long cycling (**Figure 4d** and **Figure S14**). This suggests that the NPL-polysulfide interaction is conducive to mitigating the reactivity of polysulfide by maintaining the solubility of polysulfide active materials in Li-S batteries. The high compatibility of NPL-polysulfide mixture with Li metal was further validated by immersing a Li foil in a solution of 0.5 M chemically-prepared Li_2S_6 and 0.25 M

15

NPL in DOL/DME mixture solvents. The Li foil (100 μm) was stable for 1 month maintaining its metallic luster, while the counterpart vanished in pure 0.5 M Li_2S_6 (**Figure S15**).

The complex-based NPL mediation for polysulfide oxidation.

The underlying mechanism of NPL and $LiNO_3$ additives is illustrated in **Schematic**. For the baseline electrolyte with $LiNO_3$, one primary limiting reaction of liquid Li-S electrochemistry based on S/Li_2S conversion is the long-chain polysulfide oxidation during the charge process (1).[15,23] It is elucidated that nitrate anion (NO_3^-) is susceptible to reduction to form nitrite anion (NO_2^-)[12,23] showing a Gibbs free energy of -346 KJ/mol (2), which accepts the electrons originating from (1). The overall reaction on the cathode side is likely to involve long-chain polysulfide of Li_2S_x (x=4~6) and $LiNO_3$ as sacrificial mediator, forming non-catalytic products like Li_2O (3).

$$Li_2S_x - 2e^- \longrightarrow (x/8)S_8 \quad x = 4\text{\textasciitilde}6 \tag{1}$$

$$NO_3^- + 2Li^+ + 2e^- \longrightarrow NO_2^- + 2Li_2O \quad \Delta_rG = -346.787 \text{ kJ/mol} \tag{2}$$

$$NO_3^- + Li_2S_x \longrightarrow NO_2^- + 2Li_2O + (x/8)S_8 \quad x = 4\text{\textasciitilde}6 \tag{3}$$
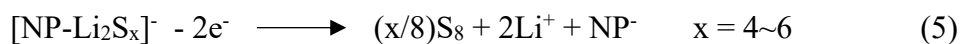
For another, polysulfide can penetrate the SEI to react Li metal causing anode degradation,[25] and it can react with the SEI components like Li_2O to form Li_xSO_y.[31] Besides, large amount of polysulfide dissolution (incomplete oxidation) leads to drastic capacity decay. Thus, the depletion of $LiNO_3$ impairs the polysulfide oxidation during charge process and deters the continual passivation of Li anode to prevent polysulfide shuttle. These attributes result in limited cycling behavior of Li-S batteries.

.
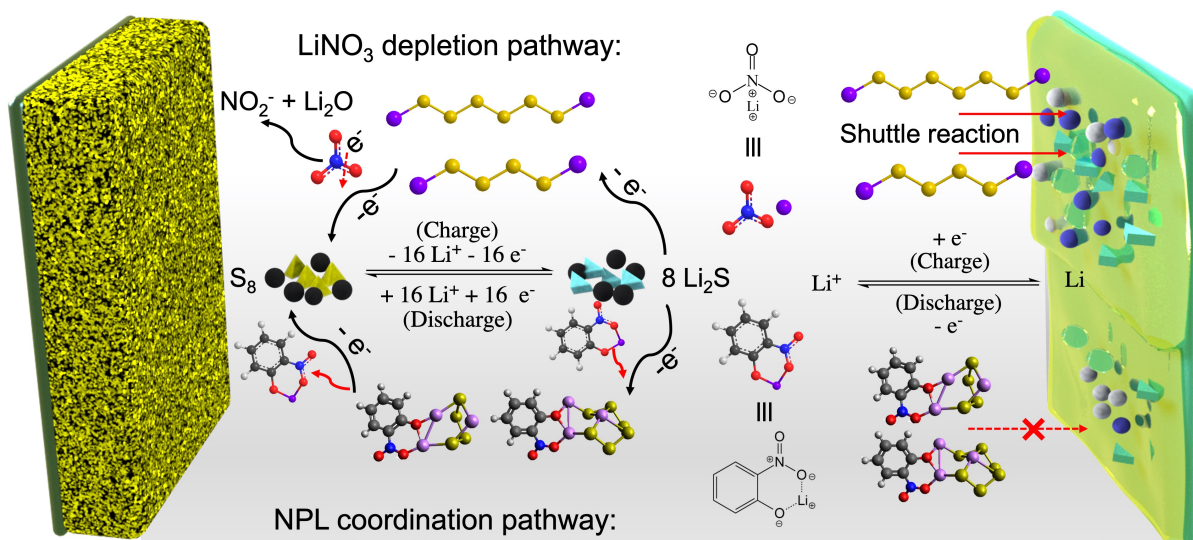
Schematic. The mechanism of Li-S electrolyte additives of NPL and $LiNO_3$.

By contrast, NPL undergoes a coordination pathway benefiting from the NPL-Li_2S_x interaction, which bypasses the decomposition of the NPL additive. According to the investigation of NPL-Li_2S_x interaction experimentally and theoretically (**Figure 3**), the lithium cation from Li_2S_x can complex with nitrophenol anion (NP$^-$) in the electrolyte (4) giving negative binding energies (**Figure 3e**). The original polysulfide is tuned to be [NP-Li_2S_4]$^-$ that undergoes subsequent oxidation into sulfur giving NP$^-$ back to the electrolyte (5), which maintains the additive reservoir during charge and discharge processes. As a result, the overall reaction remains polysulfide oxidation, without NPL depletion (1).

$$Li_2S_x + NP^- \longrightarrow [NP\text{-}Li_2S_x]^- \qquad x = 4\sim6 \qquad (4)$$

$$[NP\text{-}Li_2S_x]^- - 2e^- \longrightarrow (x/8)S_8 + 2Li^+ + NP^- \qquad x = 4\sim6 \qquad (5)$$

The non-depletable mechanism promises the NPL additive a good $LiNO_3$ alternative, supporting the liquid-state Li-S electrochemistry to take place on the S cathodes continually (good capacity retention). Besides, the NPL-Li_2S_x interaction modifies the reactivity of polysulfide, which inhibits Li corrosion by polysulfide (**Figure 1 and 2**, **Figure S15**) to maintain the anode integrity. In addition, NPL maintains the advantageous solubility of active materials of polysulfide without precipitation to lose capacity.[21] The NPL additive facilitates

polysulfide oxidation on the cathode side without being consumed. Despite this, it contributes to the passivation layer formation on the Li anode, as evidenced by the CV cathodic peaks in the first two cycles (**Figure 3a**). However, there is no continual consumption of NPL, which is conducive to extending the cycle life of Li-S batteries.

Pouch-cell validation.

Extensive research has been conducted in pursuit of high-energy-density Li-S batteries with long stability, but pouch-cells using the baseline electrolyte merely deliver limited cycle life due to series of problems.[8,19,20] Among these, the continual consumption of $LiNO_3$ has been quantitatively identified in this work and the effectiveness of our as-designed NPL additive has been further validated by pouch-cell prototyping. The electrochemical performance of single-layer pouch cells of the C-S cathode (~4 mAh cm^{-2}, 5x5 cm^2, **Figure S16**) was compared using baseline electrolyte and our NPL electrolyte, shown in **Figure 5**. The C-S cathode pouch cell delivers a higher capacity of ~100 mAh in the NPL electrolyte than ~90 mAh in the baseline electrolyte (**Figure 5a and 5c**), reflecting a high specific capacity in the NPL electrolyte (**Figure 4a** and **Figure S9**). Additionally, the Li-S pouch cell using the NPL electrolyte demonstrates an extended lifespan of approximately 80 cycles. It retains 81% of its initial capacity of about 80 mAh at 0.1 C. This contrasts obviously with counterpart cells in the baseline electrolyte, which last for less than 40 cycles at the same capacity retention, as shown in **Figure 5b and 5d**. The results demonstrate the applicability of using the NPL electrolyte and its lifespan-prolonging effect.
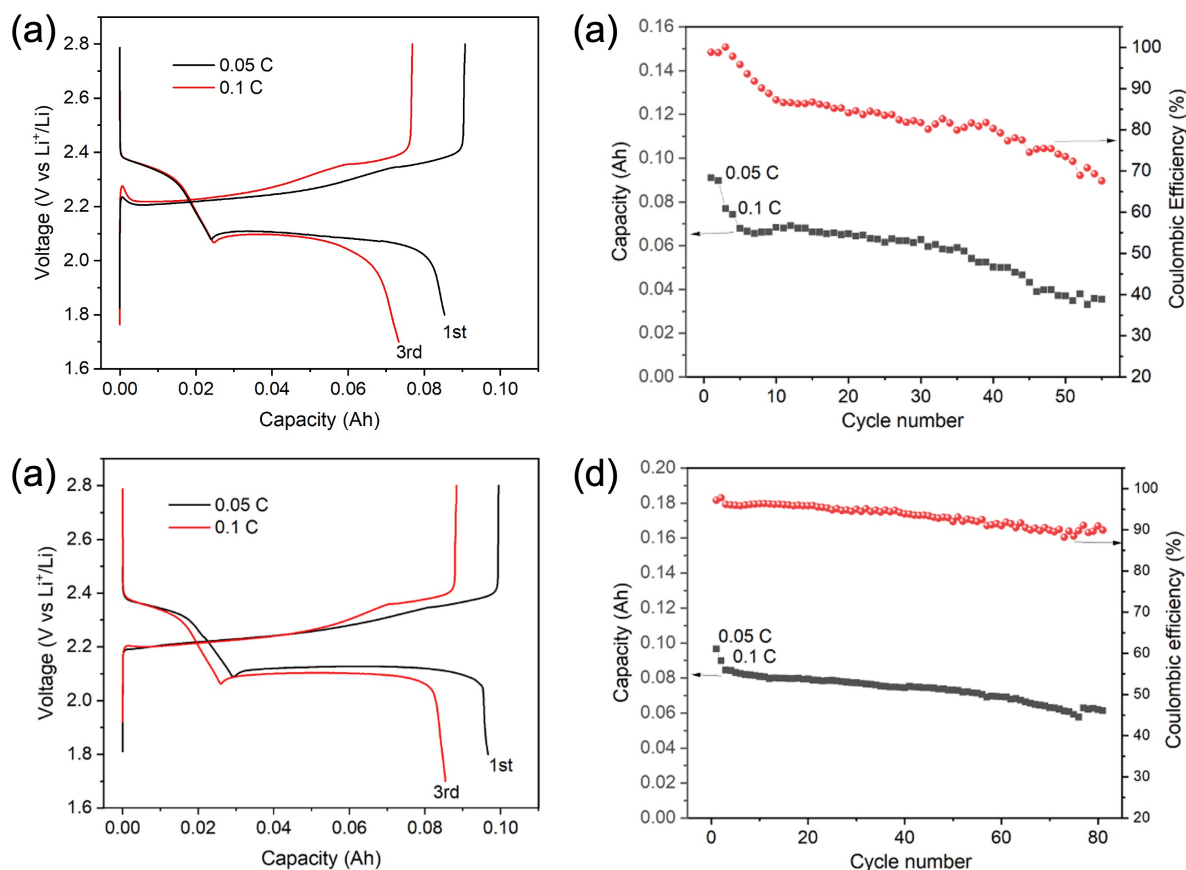
Figure 5. Electrochemical performance of single-layer pouch cells based on C-S cathodes. The voltage profiles of the pouch cells using (a) the baseline electrolyte and (c) the NPL electrolyte; The corresponding cycling stability in the baseline and NPL electrolytes (b and d). The cells consist of 100 μm Li, C-S cathode, 4.2 mg_{sulfur} cm^{-2}, 5x5 cm^2, E/S=8 μl mg_{sulfur}^{-1}, and the testing protocol started with 2 formation cycles at 0.05 C and maintained cycling at 0.1 C (1 C=1000 mA/g_{Sulfur}^{-1}).

CONCLUSION AND OUTLOOK

In this investigation, we designed and synthesized an aromatic nitro-functionalized compound of 2-nitrophenol lithium (NPL) as an additive in the electrolyte comprising 1 M LiTFSI in a DOL/DME (v/v=1:1) mixture solvent. Based on our observation, the NPL, unlike $LiNO_3$, can function as a stable additive without depleting in the electrolyte of Li-S batteries. By forming complexes with polysulfides such as Li_2S_4 and Li_2S_6, NPL can facilitate robust polysulfide oxidation during the charge process and mitigate polysulfide corrosion on the Li anode in high-energy-density Li-S batteries. Li-S batteries employing the NPL electrolyte exhibit a significantly extended lifespan of 310 cycles, contrasting with the limited 75 cycles

19

observed with baseline electrolytes containing $LiNO_3$. Furthermore, single-layer pouch cells with the NPL electrolyte display stable cycling for around 80 cycles, achieving a high capacity retention of 75%. This research suggests NPL as an alternative to $LiNO_3$, which can facilitate the development of Li-S electrolytes capable of handling high polysulfide concentrations, thus ensuring an extended lifespan for Li-S batteries.

Experimental Procedures

Resource Availability

Lead contact
Further information and requests for resources and materials should be directed to and will be fulfilled by the lead contact, Ying Shirley Meng (shirleymeng@uchicago.edu).

Materials Availability
This study generates new unique materials with a patent application number of UCSD Ref. No. SD2023-264.

Date and Code Availability
All the experimental data are presented in the paper or supplemental information.

Chemicals

Sulfur (reagent grade, Sigma Aldrich), Acetylene black and C65 (MTI), Sodium carboxymethyl cellulose (CMC binder, Sigma Aldrich, M_w = 400, 000), Lithium Metal (100 µm, Albemarle Corp, supplied by General Motors), Lithium Sulfide (Li_2S) (99.98% trace metals basis, Sigma Aldrich), Dimethoxyethane (DME) (anhydrous, 99.5%, Sigma Aldrich), 1,3-Dioxolane (anhydrous, 99.8%, Sigma Aldrich), and Lithium bis(trifluoromethane) Sulfonimide (LiTFSI) (anhydrous, 99.99% trace metals basis, Sigma Aldrich), Lithium Nitrate ($LiNO_3$) (99.99% trace metals basis), 2-nitrophenol (Sigma Aldrich), anhydrous LiOH (Sigma Aldrich), HPLC grade methanol (Fisher Scientific), and HPLC grade water (Fisher Scientific) were purchased and used.

Sample preparation

The standard solutions of $LiNO_3$: The stock solution was made by dissolving 68.95 mg $LiNO_3$ in 10 mL DME, the molar concentration was 100 mM. The standard solutions of 1 mM, 0.9 mM, 0.7 mM, 0.6 mM, and 0.5 mM were then made by diluting the stock solution. The standard solutions of NPL: The stock solution was made by dissolving 29.02 mg NPL in 2 mL DME,

https://doi.org/10.26434/chemrxiv-2024-ft9zg **ORCID:** https://orcid.org/0000-0002-7542-6108 Content not peer-reviewed by ChemRxiv. **License:** CC BY-NC-ND 4.0

the molar concentration was 100 mM. The standard solutions of 0.1 mM, 0.25 mM, 0.5 mM, 1 mM, 2 mM, and 4 mM were then made by diluting the stock solution.

Electrolyte preparation and electrochemical measurements

LiTFSI and LiNO$_3$ were dried at 130 ^{o}C for 48 h in vacuum before use. DOL and DME were dehydrated over molecular sieve (4 A$^\circ$) for overnight. The baseline electrolyte of 1 M lithium bis(trifluoromethanesulfonyl)imide (LiTFSI) and 2wt.% LiNO$_3$ in a solvent mixture of 1,3-dioxolane (DOL) and 1,2-dimethoxyethane (DME) at a 1:1 volume ratio was prepared by adding DOL/DME solvent into the weighed LiTFSI and LiNO$_3$ powder before stirring the mixture solution for 12 hours. The NPL electrolyte was prepared by adding 1 M LiTFSI DOL/DME (without LiNO$_3$) solution into the weighed NPL powder. The as-prepared NPL electrolyte is kept with Li metal immersion for another 12 hours to afford a battery grade electrolyte. The CR2032 Li-S cells were assembled using carbon-sulfur cathode (Materials synthesis, supplementary), lithium foil anode (100 µm), Celgard 2325 separator and different electrolytes. The galvanostatic discharge-charge test of coin cells was conducted on Neware instrument. The Cyclic voltammetry was performed by using a negative scan rate of 0.02 mV S^{-1} with 4 scans starting from the open circuit voltage (OCV) on Bio-Logic electrochemical workstation.

Computational Analysis

DFT binding energy calculations were performed using the Gaussian 16 package. A geometry optimization step at the B3LYP//6-31+G** level of theory was followed by single point energy calculations at the B3LYP//6-311++G** level of theory. Gibbs free energy of the reaction and Binding Energy are calculated as:

$E_{(reaction)} = E_{(products)} - E_{(reactants)}$

For the Electrostatic Potential mapping, GaussView software package was used to map the electron density between the energy levels -0.18 eV and -0.1 eV. The lithium polysulphide structures were predicted from ESP mapping and most stable structure was chosen based on the energy calculations.

Characterizations

HPLC-UV: The Thermo Scientific Vanquish quaternary pump F (VF-P20-A) coupled with the Thermo Scientific Split Sampler FT (VF-A10-A) autosampler was utilized to deliver a mobile phase through a ZORBAX Extend-C18 Column (from Agilent, C18, 4.6*50 mm, 5 µm) at a flow rate of 0.70 mL min^{-1}. The injection volume was 5 µL. For the analysis of $LiNO_3$, a binary gradient mobile phase was employed with the following gradient profile: 0 min, 0 % methanol (100% water); 10 min, 100% methanol; 12 min, 100% methanol; 15 min, 0% methanol. For NPL analysis, the gradient conditions were: 0 min, 0 % Acetonitrile (ACN) (100% water); 10 min, 100% ACN; 12 min, 100% ACN; 15 min, 0% ACN. Absorbance data for $LiNO_3$ and NPL were collected at 210 nm and 300 nm wavelengths, respectively, using the Thermo Scientific Chromeleon Chromatography Data System Software. ICP-MS (Thermo iCAP RQ single-quadrupole ICP-MS system) and HPLC-UV measurements were taken at the Environmental and Complex Analysis Laboratory (ECAL) at the University of California, San Diego.

Low-electron-dose Cryo-STEM: All cryogenic STEM characterizations were carried out using a ThermoFisher Talos 200X TEM electron microscope system operated at an accelerating voltage of 200 kV. It was fitted with Schottky X-ray FEG field emission electron gun, Gatan Continuum (1069) EELS spectrometer, STEM model, 4 in-column SDD Super-X detectors, Ceta camera and the Melbuild holder. First, Li-S cells after formations cycles at 0.05 C in the baseline and NPL electrolytes were opened in an Ar-filled glove box, and the cycled Cu TEM grids with Li metal were cleaned with DME and dried in a vacuum. The STEM (EDS Mapping) samples were transferred in ThermoFisher Talos 200X TEM with the Melbuild holder (liquid

23

N$_2$ cooling holder) under the protection of Ar atmosphere. EDS Mapping and TEM are collected at -170 °C. The EDS mapping is acquired with a probe current of around 160 pA for ~4 min.

Acknowledgements

Author Contributions

X. W. and Y. S. M. conceived the idea. X. W. and S. P. designed the experiments and contributed equally. X. W. and S. P. developed the HPLC-UV quantification methodology in this work. S. P. carried out the HPLC-UV tests and processed the data. G. R. carried out the Gaussian calculations. B. B. performed and processed the data for TGC. A. L. conducted the EIS ion conductivity test. S. B. and B. H. performed the cryogenic STEM and EDX. X. W. and B. B. performed the cryogenic FIB. X. W. and W. L. performed XPS experiment. X. W. processed

the data for XPS. X. W. synthesized the pure NPL material and prepared the NPL electrolyte. X. W. and M. M. prepared the cathodes and electrolytes. X. W. and S. W wrote the manuscript. All authors discussed the results and contributed to the manuscript. All authors have approved the final version of the manuscript.

Declaration of Interests

The authors declare no conflict of interest. This study generates new unique materials with a patent application number of UCSD Ref. No. SD2023-264.

References

1.   Larcher, D., and Tarascon, J.M. (2015). Towards greener and more sustainable batteries for electrical energy storage. Nat. Chem. *7*, 19-29. 10.1038/nchem.2085.

2.   Manthiram, A., Fu, Y., Chung, S.H., Zu, C., and Su, Y.S. (2014). Rechargeable lithium-sulfur batteries. Chem. Rev. *114*, 11751-11787. 10.1021/cr500062v.

3.   Zhao, M., Li, B.Q., Zhang, X.Q., Huang, J.Q., and Zhang, Q. (2020). A Perspective toward Practical Lithium-Sulfur Batteries. ACS Cent. Sci. *6*, 1095-1104. 10.1021/acscentsci.0c00449.

4.   Shao, Q., Zhu, S., and Chen, J. (2023). A review on lithium-sulfur batteries: Challenge, development, and perspective. Nano Res. *16*, 8097-8138. 10.1007/s12274-022-5227-0.

5.   Lv, D., Zheng, J., Li, Q., Xie, X., Ferrara, S., Nie, Z., Mehdi, L.B., Browning, N.D., Zhang, J.-G., Graff, G.L., et al. (2015). High Energy Density Lithium-Sulfur Batteries: Challenges of Thick Sulfur Cathodes. Advanced Energy Materials *5*. 10.1002/aenm.201402290.

6.   Pan, H., Chen, J., Cao, R., Murugesan, V., Rajput, N.N., Han, K.S., Persson, K., Estevez, L., Engelhard, M.H., Zhang, J.-G., et al. (2017). Non-encapsulation approach for high-performance Li–S batteries through controlled nucleation and growth. Nat. Energy *2*, 813-820. 10.1038/s41560-017-0005-z.

7.   Wang, X., Yang, Y., Lai, C., Li, R., Xu, H., Tan, D.H.S., Zhang, K., Yu, W., Fjeldberg, O., Lin, M., et al. (2021). Dense-Stacking Porous Conjugated Polymer as Reactive-Type Host for High-Performance Lithium Sulfur Batteries. Angew. Chem. Int. Ed. *60*, 11359-11369. 10.1002/anie.202016240.

8.   Zhao, C., Xu, G.L., Yu, Z., Zhang, L., Hwang, I., Mo, Y.X., Ren, Y., Cheng, L., Sun, C.J., Ren, Y., et al. (2021). A high-energy and long-cycling lithium-sulfur pouch cell

via a macroporous catalytic cathode with double-end binding sites. Nat. Nanotechnol. *16*, 166-173. 10.1038/s41565-020-00797-w.

9.   Wang, M., Emre, A.E., Kim, J.Y., Huang, Y., Liu, L., Cecen, V., Huang, Y., and Kotov, N.A. (2022). Multifactorial engineering of biomimetic membranes for batteries with multiple high-performance parameters. Nat. Commun. *13*, 278. 10.1038/s41467-021-27861-w.

10. Zhang, K., Liu, W., Gao, Y., Wang, X., Chen, Z., Ning, R., Yu, W., Li, R., Li, L., Li, X., et al. (2021). A High-Performance Lithium Metal Battery with Ion-Selective Nanofluidic Transport in a Conjugated Microporous Polymer Protective Layer. Adv. Mater. *33*, e2006323. 10.1002/adma.202006323.

11. Tang, W., Yin, X., Kang, S., Chen, Z., Tian, B., Teo, S.L., Wang, X., Chi, X., Loh, K.P., Lee, H.W., and Zheng, G.W. (2018). Lithium Silicide Surface Enrichment: A Solution to Lithium Metal Battery. Adv. Mater., e1801745. 10.1002/adma.201801745.

12. Liu, Y., Elias, Y., Meng, J., Aurbach, D., Zou, R., Xia, D., and Pang, Q. (2021). Electrolyte solutions design for lithium-sulfur batteries. Joule *5*, 2323-2364. 10.1016/j.joule.2021.06.009.

13. Barghamadi, M., Best, A.S., Bhatt, A.I., Hollenkamp, A.F., Musameh, M., Rees, R.J., and Rüther, T. (2014). Lithium–sulfur batteries—the solution is in the electrolyte, but is the electrolyte a solution? Energy Environ. Sci. *7*, 3902-3920. 10.1039/c4ee02192d.

14. Tarquini, G., Dell'Era, A., Prosini, P.P., Scaramuzzo, F.A., Lupi, C., and Pasquali, M. (2020). Polysulfide solution effects on Li S batteries performances. J. Electroanal. Chem. *870*. 10.1016/j.jelechem.2020.114239.

15. Zhang, S.S. (2016). A new finding on the role of $LiNO_3$ in lithium-sulfur battery. J. Power Sources *322*, 99-105. 10.1016/j.jpowsour.2016.05.009.

16.	Rosenman, A., Elazari, R., Salitra, G., Markevich, E., Aurbach, D., and Garsuch, A. (2015). The Effect of Interactions and Reduction Products of $LiNO_3$, the Anti-Shuttle Agent, in Li-S Battery Systems. J. Electrochem. Soc. *162*, A470-A473. 10.1149/2.0861503jes.

17.	Tan, J., Ye, M., and Shen, J. (2022). Deciphering the role of $LiNO_3$ additives in Li-S batteries. Mater. Horiz. *9*, 2325-2334. 10.1039/d2mh00469k.

18.	Peng, H.-J., Huang, J.-Q., Cheng, X.-B., and Zhang, Q. (2017). Review on High-Loading and High-Energy Lithium-Sulfur Batteries. Adv. Energy Mater. *7*. 10.1002/aenm.201700260.

19.	Xie, J., Sun, S.Y., Chen, X., Hou, L.P., Li, B.Q., Peng, H.J., Huang, J.Q., Zhang, X.Q., and Zhang, Q. (2022). Fluorinating the Solid Electrolyte Interphase by Rational Molecular Design for Practical Lithium-Metal Batteries. Angew. Chem. Int. Ed. *61*, e202204776. 10.1002/anie.202204776.

20.	Hou, L.P., Yao, N., Xie, J., Shi, P., Sun, S.Y., Jin, C.B., Chen, C.M., Liu, Q.B., Li, B.Q., Zhang, X.Q., and Zhang, Q. (2022). Modification of Nitrate Ion Enables Stable Solid Electrolyte Interphase in Lithium Metal Batteries. Angew. Chem. Int. Ed. *61*, e202201406. 10.1002/anie.202201406.

21.	Yang, T., Qian, T., Liu, J., Xu, N., Li, Y., Grundish, N., Yan, C., and Goodenough, J.B. (2019). A New Type of Electrolyte System To Suppress Polysulfide Dissolution for Lithium-Sulfur Battery. ACS Nano *13*, 9067-9073. 10.1021/acsnano.9b03304.

22.	Yu, L., Ong, S.J.H., Liu, X., Mandler, D., and Xu, Z.J. (2021). The importance of the dissolution of polysulfides in lithium-sulfur batteries and a perspective on high-energy electrolyte/cathode design. Electrochim. Acta *392*. 10.1016/j.electacta.2021.139013.

23. Jozwiuk, A., Berkes, B.B., Weiß, T., Sommer, H., Janek, J., and Brezesinski, T. (2016). The critical role of lithium nitrate in the gas evolution of lithium–sulfur batteries. Energy & Environ. Sci. *9*, 2603-2608. 10.1039/c6ee00789a.

24. Fang, C., Li, J., Zhang, M., Zhang, Y., Yang, F., Lee, J.Z., Lee, M.H., Alvarado, J., Schroeder, M.A., Yang, Y., et al. (2019). Quantifying inactive lithium in lithium metal batteries. Nature *572*, 511-515. 10.1038/s41586-019-1481-z.

25. Nanda, S., and Manthiram, A. (2020). Lithium degradation in lithium–sulfur batteries: insights into inventory depletion and interphasial evolution with cycling. Energy & Environ. Sci. *13*, 2501-2514. 10.1039/d0ee01074j.

26. Lu, B., Li, W., Cheng, D., Bhamwala, B., Ceja, M., Bao, W., Fang, C., and Meng, Y.S. (2022). Suppressing Chemical Corrosions of Lithium Metal Anodes. Adv. Energy Mater. *12*. 10.1002/aenm.202202012.

27. Zhang, Q.-K., Zhang, X.-Q., Wan, J., Yao, N., Song, T.-L., Xie, J., Hou, L.-P., Zhou, M.-Y., Chen, X., Li, B.-Q., et al. (2023). Homogeneous and mechanically stable solid–electrolyte interphase enabled by trioxane-modulated electrolytes for lithium metal batteries. Nat. Energy *8*, 725-735. 10.1038/s41560-023-01275-y.

28. Aurbach, D., Pollak, E., Elazari, R., Salitra, G., Kelley, C.S., and Affinito, J. (2009). On the Surface Chemical Aspects of Very High Energy Density, Rechargeable Li-Sulfur Batteries. J. Electrochem. Soc. *156*, A694-A702. 10.1149/1.3148721.

29. Wu, D.S., Shi, F., Zhou, G., Zu, C., Liu, C., Liu, K., Liu, Y., Wang, J., Peng, Y., and Cui, Y. (2018). Quantitative investigation of polysulfide adsorption capability of candidate materials for Li-S batteries. Energy Stor. Mater. *13*, 241-246. 10.1016/j.ensm.2018.01.020.

30. Ali, H.S.H.M., Anwar, Y., and Khan, S.A. (2021). Vigna radiata Impregnated Zero-Valent CuAg NPs: Applications in Nitrophenols Reduction, Dyes Discoloration and Antibacterial Activity. J. Cluster Sci. *33*, 1407-1416. 10.1007/s10876-021-02067-8.

31. Diao, Y., Xie, K., Xiong, S., and Hong, X. (2013). Shuttle phenomenon – The irreversible oxidation mechanism of sulfur active material in Li–S battery. J. Power Sources *235*, 181-186. 10.1016/j.jpowsour.2013.01.132.